Journal of Sound and Vibration (2002) **254**(2), 203–218
doi:10.1006/jsvi.2001.4045. available online at http://www.idealibrary.com on IDEAL®

MICRO-SENSING CHARACTERISTICS AND MODAL VOLTAGES OF LINEAR/NON-LINEAR TOROIDAL SHELLS

H. S. Tzou and D. W. Wang

Department of Mechanical Engineering, Structronics Lab., University of Kentucky, Lexington, KY 40506-0108, *U.S.A.*

(*Received* 26 *February* 2001, *and in final form* 10 *September* 2001)

Toroidal shells belong to the shells of revolution family. Dynamic sensing signals and their distributed characteristics of spatially distributed sensors or neurons laminated on thin toroidal shell structures are investigated in this study. Spatially distributed modal voltages and signal patterns are related to the meridional and circumferential membrane/bending strains, based on the direct piezoelectricity, the Gauss theorem, the Maxwell principle and the open-circuit assumption; linear and non-linear toroidal shells are defined based on the thin shell theory and the von Karman geometric non-linearity. With the simplified mode shape functions defined by the Donnell–Mushtari–Vlasov theory, modal-dependent distributed signals and detailed signal components of spatially distributed sensors or neurons are defined and these signals are quantitatively illustrated. Signal distributions basically reveal distinct modal characteristics of toroidal shells. Parametric studies suggest that the dominating signal component results from the meridional membrane strains. Shell dimensions, materials, boundary conditions, natural modes, sensor locations/distributions/sizes, modal strain components, etc., all influence the spatially distributed modal voltages and signal generations.

1. INTRODUCTION

Toroidal shell structures and components are often proposed for space telescopes, inflatable space structures, neutron accelerators, space colonies, cooling tubes, etc., over the years. Effective distributed control of these toroidal shell structures can enhance their operation precision, accuracy, and reliability. Static, dynamic, vibration, and buckling characteristics of toroidal shells have been studied [1–5]. Stress and free-vibration analyses of pipe-type toroidal shells have also been investigated recently [6–8].

Precision maneuver and control of shells requires thorough understanding of not only the dynamic behavior, but also the distributed sensing characteristics serving as performance indices or feedback signals [9]. Distributed sensing characteristics of distributed segmented sensors and spatially shaped orthogonal sensors of cylindrical shells and rings have been evaluated recently [10–12]. This study is to evaluate distributed sensing characteristics of linear and non-linear toroidal shells of revolution laminated with spatially distributed piezoelectric sensors of neurons. Mathematical modelling of a generic toroidal shell of revolution is presented first, followed by distributed sensing of toroidal shells with spatially distributed sensors. Due to the complexity of the original toroidal shells, exact solutions are difficult to derive. Thus, the Donnell–Mushtari–Vlasov theory is employed and, thus, a set of mode shape functions can be assumed and distributed sensor signals can be defined. Detailed spatially distributed sensing signals and modal voltages are presented in case studies.

0022-460X/02/$35.00

2. MATHEMATICAL MODELLING

A thin toroidal shell of revolution and its cross-section are shown in Figure 1 where $\alpha_1 = \phi$ denotes the meridional co-ordinate and $\alpha_2 = \psi$ denotes the circumferential co-ordinate respectively. For convenience, a secondary circumferential co-ordinate χ is adopted as $\chi = R\psi/r$, where R is the toroidal shell (major) radius and r is the shell cross-sectional radius. Assume that the toroidal shell is thin (with thickness h), and thus follow the Love–Kirchhoff thin shell theory and assumptions. Mathematical models of the linear and non-linear toroidal shells are defined first, followed by the Donnell–Mushtari–Vlasov simplifications.

Furthermore, a spatially distributed sensor layer (with thickness h^s) is laminated to the shell surface and it is much thinner than the elastic shell, i.e., $h \gg h^s$. Thus, the influence of sensor elastic properties on the elastic toroidal shell dynamics is neglected. The distributed sensor layer responds to the dynamic oscillations and generates signals. The sensor layer can be further discretized into spatially distributed infinitesimal "neurons" revealing microscopic distributed local signals of the toroidal shells. These spatially distributed signals and modal voltages are investigated in this study.

The Lamé parameters and curvature radii of toroidal shells of revolution are

$$A_1 = r, \quad A_2 = r\xi, \quad R_1 = r, \quad R_2 = r\xi/(\gamma \cos\phi), \tag{1}$$

where $\xi = 1 + \gamma \cos\phi$ and $\gamma = r/R$. The membrane and bending strains (s°_{ij} and k_{ij}) of the toroidal shells are functions of displacements u_i:

$$s^\circ_{\phi\phi} = \frac{1}{r}\left(\frac{\partial u_\phi}{\partial \phi} + u_3\right), \qquad s^\circ_{\chi\chi} = \frac{1}{r\xi}\left(-u_\phi \sin\phi + \frac{\partial u_\chi}{\partial \chi} + u_3 \gamma \cos\phi\right), \tag{2,3}$$

$$s^\circ_{\phi\chi} = \frac{1}{r\xi}\left(\frac{\partial u_\phi}{\partial \chi} + u_\chi \gamma \sin\phi\right) + \frac{1}{r}\frac{\partial u_\chi}{\partial \phi}, \qquad k_{\phi\phi} = \frac{1}{r^2}\left(\frac{\partial u_\phi}{\partial \phi} - \frac{\partial^2 u_3}{\partial \phi^2}\right), \tag{4,5}$$

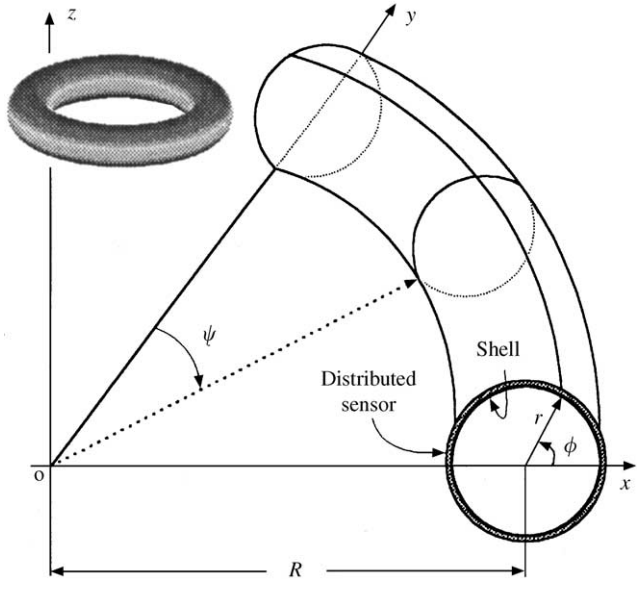

Figure 1. A toroidal shell of revolution with a distribute sensor layer (not to scale).

$$k_{\chi\chi} = -\frac{\sin\phi}{rR\xi}\left(u_\phi - \frac{\partial u_3}{\partial\phi}\right) + \frac{\cos\phi}{rR\xi^2}\frac{\partial u_\chi}{\partial\chi} - \frac{1}{(r\xi)^2}\frac{\partial^2 u_3}{\partial\chi^2}, \tag{6}$$

$$k_{\phi\chi} = \frac{1}{r^2\xi}\frac{\partial u_\phi}{\partial\chi} + \frac{\cos\phi}{rR\xi}\frac{\partial u_\chi}{\partial\phi} + \frac{u_\chi}{(R\xi)^2}\sin\phi\cos\phi - \frac{1}{r^2\xi}\frac{\partial^2 u_3}{\partial\phi\partial\chi} - \frac{\sin\phi}{rR\xi^2}\frac{\partial u_3}{\partial\chi}. \tag{7}$$

The total strains S_{ij} are the summation of the membrane strain and the bending strain:

$$S_{\phi\phi} = s^\circ_{\phi\phi} + \alpha_3 k_{\phi\phi}, \quad S_{\chi\chi} = s^\circ_{\chi\chi} + \alpha_3 k_{\chi\chi}, \quad S_{\phi\chi} = s^\circ_{\phi\chi} + \alpha_3 k_{\phi\chi}, \tag{8-10}$$

where α_3 denotes the location measured from the shell neutral surface. These strain–displacement relations will be used in the signal–displacement equation of spatially distributed sensors and neurons later. Following the thin shell assumptions, the rotation angles are defined as $\beta_\phi = (1/r)(u_\phi - \partial u_3/\partial\phi)$ and $\beta_\chi = (1/r\xi)(u_\chi\gamma\cos\phi - \partial u_3/\partial\chi)$. For *non-linear* toroidal shells with geometric non-linearity defined by the von Karman geometric *non-linearity*, the membrane strains need to include the quadratic effect of the transverse displacement [13]:

$$s^\circ_{\phi\phi} = \frac{1}{r}\left(\frac{\partial u_\phi}{\partial\phi} + u_3\right) + \frac{1}{2}\left(\frac{\partial u_3}{\partial\phi}\right)^2, \tag{11}$$

$$s^\circ_{\chi\chi} = \frac{1}{r\xi}\left(-u_\phi\gamma\sin\phi + \frac{\partial u_\chi}{\partial\chi} + u_3\gamma\cos\phi\right) + \frac{1}{2}\left(\frac{\partial u_3}{\partial\chi}\right)^2. \tag{12}$$

The resulting membrane forces N_{ij} and moments M_{ij} are defined as functions of membrane strains $s_{ij}{}^\circ$ and bending strains k_{ij}:

$$N_{\phi\phi} = K(s^\circ_{\phi\phi} + \mu s^\circ_{\chi\chi}), \quad N_{\chi\chi} = K(s^\circ_{\chi\chi} + \mu s_{\phi\phi}), \quad N_{\phi\chi} = N_{\chi\phi} = \frac{K(1-\mu)}{2}s^\circ_{\phi\chi}, \tag{13-15}$$

$$M_{\phi\phi} = D(k_{\phi\phi} + \mu k_{\chi\chi}), \quad M_{\chi\chi} = D(k_{\chi\chi} + \mu k_{\phi\phi}), \quad M_{\phi\chi} = M_{\chi\phi} = \frac{D(1-\mu)}{2}k_{\phi\chi}, \tag{16-18}$$

where the membrane stiffness K and the bending stiffness D are, respectively, defined as $K = Yh/(1-\mu^2)$ and $D = Yh^3/[12(1-\mu^2)]$ and Y is the modulus of elasticity, μ is the Poisson ratio. Accordingly, the system equations of the thin toroidal shells in three axial directions are, respectively, defined as follows:

$$-r\xi\frac{\partial N_{\phi\phi}}{\partial\phi} + r\gamma(N_{\phi\phi} - N_{\chi\chi})\sin\phi - r\frac{\partial N_{\chi\phi}}{\partial\chi} - r\xi Q_{\phi 3} + r^2\xi\rho h\ddot{u}_\phi = r^2\xi q_\phi, \tag{19}$$

$$-r\xi\frac{\partial N_{\phi\chi}}{\partial\phi} + 2r\gamma N_{\phi\chi}\sin\phi - r\frac{\partial N_{\chi\chi}}{\partial\chi} - r\gamma Q_{\chi 3}\cos\phi + r^2\xi\rho h\ddot{u}_\chi = r^2\xi q_\chi, \tag{20}$$

$$-r\xi\frac{\partial Q_{\phi 3}}{\partial\phi} + r\gamma Q_{\phi 3}\sin\phi - r\frac{\partial Q_{\chi 3}}{\partial\chi} + r\xi N_{\phi\phi} + r\gamma N_{\chi\chi}\cos\phi + r^2\xi\rho h\ddot{u}_3 = r^2\xi q_3, \tag{21}$$

where ρ is the mass density; $\ddot{u}_i$ is the acceleration; q_i is the external excitation; and the transverse shear effects Q_{ij} are defined as functions of moments:

$$Q_{\phi 3} = \frac{1}{r\xi}\left[\xi\frac{\partial M_{\phi\chi}}{\partial\phi} + \gamma(M_{\chi\chi} - M_{\phi\phi})\sin\phi + \frac{\partial M_{\chi\phi}}{\partial\chi}\right], \tag{22}$$

$$Q_{\chi 3} = \frac{1}{r\xi}\left[\xi\frac{\partial M_{\phi\chi}}{\partial\phi} - 2\gamma M_{\phi\chi}\sin\phi + \frac{\partial M_{\chi\chi}}{\partial\chi}\right]. \tag{23}$$

As discussed previously, exact analytical solutions of thin toroidal shells of revolutions are difficult to obtain. Thus, simplification theories are often employed and simplified

analytical solutions are derived. In this study, the Donnell–Mushtari–Vlasov simplification theory is used. There are three fundamental assumptions in the Donnell–Mushtari–Vlasov approximation: (1) in-plane displacements can be neglected in the bending strain expressions, but not in the membrane strain expressions; (2) in-plane inertia forces can be neglected, i.e., $\rho h\ddot{u}_k \cong 0$, $k = \phi, \psi$; and (3) the transverse shear effects, i.e., Q_{31}/R_1 and Q_{32}/R_2, in the transverse equations can be neglected. Based on the first assumption, one can simplify the bending strain–displacement equations:

$$k_{\phi\phi} = -\frac{1}{r^2}\frac{\partial^2 u_3}{\partial\phi^2}, \quad k_{\chi\chi} = \frac{\sin\phi}{rR\xi}\frac{\partial u_3}{\partial\phi} - \frac{1}{(r\xi)^2}\frac{\partial^2 u_3}{\partial\chi^2}, \quad k_{\phi\chi} = -\frac{1}{r^2\xi}\frac{\partial^2 u_3}{\partial\phi\partial\chi} - \frac{\sin\phi}{rR\xi^2}\frac{\partial u_3}{\partial\chi}. \tag{24-26}$$

Based on the second and third assumptions, the influence of in-plane inertia forces is neglected and the transverse shear terms are also neglected. Thus, the simplified system equations based on the Donnell–Mushtari–Vlasov theory become

$$-r\xi\frac{\partial N_{\phi\phi}}{\partial\phi} + r\gamma(N_{\phi\phi} - N_{\chi\chi})\sin\phi - r\frac{\partial N_{\chi\phi}}{\partial\chi} = 0, \tag{27}$$

$$-r\xi\frac{\partial N_{\phi\chi}}{\partial\phi} + 2r\gamma N_{\phi\chi}\sin\phi - r\frac{\partial N_{\chi\chi}}{\partial\chi} = 0, \tag{28}$$

$$r\xi D\nabla^4 u_3 + \xi N_{\phi\phi} + N_{\chi\chi}\gamma\cos\phi + r\xi\rho h\ddot{u}_3 = r\xi q_3, \tag{29}$$

where

$$\nabla^2(\cdot) = \frac{1}{r^2\xi}\left[\frac{\partial}{\partial\phi}\left(\xi\frac{\partial(\cdot)}{\partial\phi}\right) + \frac{\partial}{\partial\chi}\left(\frac{1}{\xi}\frac{\partial(\cdot)}{\partial\chi}\right)\right].$$

A set of assumed mode shape functions based on the simplified theory are then defined and used in the modal signal–displacement expressions next.

3. DISTRIBUTED SENSING AND MODAL VOLTAGES

The spatially distributed piezoelectric sensor layer responds to dynamic strains and generates electrical signals, due to the direct piezoelectric effect. Based on the modal expansion concept, the displacement is composed of all participating modes. Thus, the sensor signals are also functions of modal-dependent strains. In this section, mode shape functions are defined first, followed by modal-dependent signals—modal voltages. Based on the Gauss theory, Maxwell's principle and the open-voltage assumption, the sensor signal ϕ^s of a generic shell sensor can be expressed as [9,14]

$$\phi^s = \frac{h^s}{S^e}\int_{S^e}(h_{31}S_{11} + h_{32}S_{22} + h_{36}S_{12})\,\mathrm{d}S^e, \tag{30}$$

where S^e is the effective sensor area, h^s is the sensor thickness, S_{11} and S_{22} are the normal strains, S_{12} is the in-plane shear strain, and h_{31}, h_{32} and h_{36} are the piezoelectric (displacement) constants. Note that $h_{31} = h_{32}$ and $h_{36} = 0$ for most commercial piezoelectric materials. (Note that since the in-plane electric fields are negligible for most widely used piezoelectric materials, e.g., polyvinylidene fluoride (PVDF), the sensing signals resulting from the in-plane electric fields are not considered here. However, it has been reported that, for some specific piezoelectric structures, the in-plane electric field could be more significant than the through-the-thickness electric field and the through-thickness electric potential is not linear even in the case of a thin-walled structure [15,16].)

Expanding the surface integration and using the toroidal shell parameters yields

$$\phi^s = \frac{h^s}{S^e}\int_{S^e}(h_{31}S^s_{11} + h_{32}S^s_{22})A_1A_2\,\mathrm{d}\alpha_1\,\mathrm{d}\alpha_2, \tag{31a}$$

$$\phi^s(\phi,\psi) = \frac{h^s}{S^e}\int_{\phi}\int_{\psi}(h_{31}S^s_{\phi\phi} + h_{32}S^s_{\psi\psi})r^2(1+\gamma\cos\phi)\,\mathrm{d}\phi\,\mathrm{d}\psi, \tag{31b}$$

where the superscript "s" denotes the sensor-related properties. A_1 and A_2 are the Lamé parameters, α_1 and α_2 are the two curvilinear co-ordinates. The mode shape functions (or the displacement fields) U_i $(i = \phi, \psi, 3)$ defined in the modal domain of the shear-diaphragm-supported toroidal shells following the Donnell–Mushtari–Vlasov approximation are [8]

$$U_\phi = \sum_{m=1}^{\infty}\sum_{n=1}^{\infty}A_{mn}\sin(m\phi)\sin\left(\frac{n\pi\psi}{\psi^*}\right), \tag{32a}$$

$$U_\psi = \sum_{m=1}^{\infty}\sum_{n=1}^{\infty}B_{mn}\cos(m\phi)\cos\left(\frac{n\pi\psi}{\psi^*}\right), \tag{32b}$$

$$U_3 = \sum_{m=1}^{\infty}\sum_{n=1}^{\infty}C_{mn}\cos(m\phi)\sin\left(\frac{n\pi\psi}{\psi^*}\right), \tag{32c}$$

where A_{mn}, B_{mn}, and C_{mn} are the modal oscillation amplitudes, ψ^* defines the circumferential angle $(2\pi \geqslant \psi^* > 0)$, and m (meridional), n (circumferential) are the mode (or half-wave) numbers, $m, n = 1, 2, \ldots$. (Note that the rigid body mode has no strain variations and thus there is no signal generation associated with the rigid body mode, although there exists a rigid mode for a totally free toroidal shell.) Thus, the mnth mode shape functions of the shear-diaphragm-supported toroidal shells are $U_\phi(m,n) = A_{mn}\sin(m\phi)\sin(n\pi\psi/\psi^*)$, $U_\psi(m,n) = B_{mn}\cos(m\phi)\cos(n\pi\psi/\psi^*)$, and $U_3(m,n) = C_{mn}\cos(m\phi)\sin(n\pi\psi/\psi^*)$ respectively. For convenience, the subscripts m and n associated with the modal amplitudes are neglected in the following derivations. Note that the mode shape functions satisfy the so-called shear-diaphragm boundary condition analogous to the simply supported boundary condition of a simple beam [8,17].

Recall that the distributed sensor layer is surface laminated and its mid-plane distance measured from the shell neutral surface is $r^s_1 = r^s_2 = (h + h^s)/2$. Accordingly, toroidal shell strains $S_{\phi\phi}(m,n) = s^{\circ}_{\phi\phi} + \alpha_3 k_{\phi\phi}$ and $S_{\psi\psi}(m,n) = s^{\circ}_{\psi\psi} + \alpha_3 k_{\psi\psi}$ defined by the modal amplitudes are respectively written as

$$s^{\circ}_{\phi\phi}(m,n) = \frac{(mA + C)}{r}\sin\left(\frac{n\pi\psi}{\psi^*}\right)\cos(m\phi), \quad k_{\phi\phi}(m,n) = \frac{(m^2C)}{r^2}\sin\left(\frac{n\pi\psi}{\psi^*}\right)\cos(m\phi), \tag{33-34}$$

$$s^{\circ}_{\psi\psi}(m,n) = \frac{1}{r\xi}\left[-A\gamma\sin(m\phi)\sin\phi - B\left(\frac{n\pi\gamma}{\psi^*}\right)\cos(m\phi) + C\gamma\cos(m\phi)\cos\phi\right]\sin\left(\frac{n\pi\psi}{\psi^*}\right), \tag{35}$$

$$K_{\psi\psi}(m,n) = \left\{-\frac{mC}{rR\xi}\sin(m\phi)\sin\phi + \frac{C}{(r\xi)^2}\left(\frac{n\pi\gamma}{\psi^*}\right)^2\cos(m\phi)\right\}\sin\left(\frac{n\pi\psi}{\psi^*}\right). \tag{36}$$

Since the sensor layer is thin and surface laminated, the strains in the sensor layer are equal to the outermost surface strains of the toroidal shell. Imposing the

Donell–Mushtari–Vlasov assumption and including the sensor location effect yields the strain-mode shape function relations and the sensor signal equation of the distributed sensor layer laminated on the toroidal thin shell:

$$S^s_{\phi\phi}(m,n) = \left[\frac{(mA+C)}{r} + \frac{(h+h^s)(m^2C)}{2r^2}\right] \sin\left(\frac{n\pi\psi}{\psi^*}\right) \cos(m\phi), \tag{37}$$

$$\begin{aligned} S^s_{\psi\psi}(m,n) = \Bigg\{ & \left[-\frac{A\gamma}{r\xi} - \frac{(h+h^s)(mC)}{2rR\xi}\right] \sin(m\phi)\sin\phi \\ & + \left[-B\left(\frac{n\pi\gamma}{\psi^*}\right) + \frac{C(h+h^s)}{2(r\xi)^2}\left(\frac{n\pi\gamma}{\psi^*}\right)^2\right] \cos(m\phi) \\ & + C\gamma\cos(m\phi)\cos\phi \Bigg\} \sin\left(\frac{n\pi\psi}{\psi^*}\right), \end{aligned} \tag{38}$$

$$\begin{aligned} \phi^s_{mn}(\phi,\psi) = & \frac{h^s}{S^e}\int_\phi\int_\psi \Bigg\{ h_{31}\left[\left[\frac{(mA+C)}{r} + \frac{(h+h^s)(m^2C)}{2r^2}\right] \sin\left(\frac{n\pi\psi}{\psi^*}\right)\cos(m\phi)\right] \\ & + h_{32}\Bigg[\Bigg(\left[-\frac{A\gamma}{r\xi} - \frac{(h+h^s)(mC)}{2rR\xi}\right] \sin(m\phi)\sin\phi \\ & + \left[-B\left(\frac{n\pi\gamma}{\psi^*}\right) + \frac{C(h+h^s)}{2(r\xi)^2}\left(\frac{n\pi\gamma}{\psi^*}\right)^2\right] \cos(m\phi) \\ & + C\gamma\cos(m\phi)\cos\phi\Bigg) \sin\left(\frac{n\pi\psi}{\psi^*}\right)\Bigg]\Bigg\} r^2(1+\gamma\cos\phi)\,\mathrm{d}\phi\,\mathrm{d}\psi. \end{aligned} \tag{39}$$

4. ANALYSIS OF DISTRIBUTED SIGNAL COMPONENTS

Note that the sensing signals defined previously are the distributed signals integrated over the whole sensor area S^e and averaged over the sensor area, due to instantaneous charge distribution and averaging on the sensor surface. Accordingly, only the "averaged" spatial effect is displayed. In order to study microscopic signal–strain relations, the sensor electrodes are assumed infinitesimally small—"sensor neurons" and thus local signal distributions can be revealed. Spatial modal voltage distributions can be established by plotting all local neuron signals $\phi^s_{mn}(\phi^*_a, \psi^*_a)$, where "*" denotes a specified neuron location "a":

$$\begin{aligned} \phi^s_{mn}(\phi^*_a,\psi^*_a) = h^s\Bigg\{ & h_{31}\left[\left[\frac{(mA+C)}{r} + \frac{(h+h^s)(m^2C)}{2r^2}\right] \sin\left(\frac{n\pi\psi}{\psi^*}\right)\cos(m\phi)\right] \\ & + h_{32}\Bigg[\Bigg(\left[-\frac{A\gamma}{r\xi} - \frac{(h+h^s)(mC)}{2rR\xi}\right] \sin(m\phi)\sin\phi \\ & + \left[-B\left(\frac{n\pi\gamma}{\psi^*}\right) + \frac{C(h+h^s)}{2(r\xi)^2}\left(\frac{n\pi\gamma}{\psi^*}\right)^2\right] \cos(m\phi) \\ & + C\gamma\cos(m\phi)\cos\phi\Bigg) \sin\left(\frac{n\pi\psi}{\psi^*}\right)\Bigg]\Bigg\}. \end{aligned} \tag{40}$$

Thus, the total signal is $[\phi^s_{mn}(\phi^*_a, \psi^*_a)] = [\phi^s_{mn}(\phi^*_a, \psi^*_a)]_{men} + [\phi^s_{mn}(\phi^*_a, \psi^*_a)]_{bend}$, where the subscripts "*men*" and "*bend*" denote the membrane and the bending effects respectively. The modal sensing signals $[\phi^s_{mn}(\phi^*_a, \psi^*_a)]_{men}$ induced by the membrane strains and $[\phi^s_{mn}(\phi^*_a, \psi^*_a)]_{bend}$ induced by the bending strains are, respectively, defined as

$$[\phi^s_{mn}(\phi^*_a, \psi^*_a)]_{men} = h^s(h_{31}s^{\circ}_{\phi\phi} + h_{32}s^{\circ}_{\psi\psi}) = h^s\left\{h_{31}\frac{(mA+C)}{r}\sin\left(\frac{n\pi\psi}{\psi^*}\right)\cos(m\phi) + h_{32}\frac{1}{r\xi}\left[-A\gamma\sin(m\phi)\sin\phi - B\left(\frac{n\pi\gamma}{\psi^*}\right)\cos(m\phi) + C\gamma\cos(m\phi)\cos\phi\right]\sin\left(\frac{n\pi\psi}{\psi^*}\right)\right\}, \tag{41}$$

$$[\phi^s_{mn}(\phi^*_a, \psi^*_a)]_{bend} = h^s(h_{31}r^s_1k_{\phi\phi} + h_{32}r^s_2k_{\psi\psi}) \quad \text{with} \quad r^s_1 = r^s_2 = \tfrac{1}{2}(h+h^s), \tag{42}$$

$$[\phi^s_{mn}(\phi^*_a, \psi^*_a)]_{bend} = \frac{h^s(h+h^s)}{2}\left\{h_{31}\frac{(m^2C)}{r^2}\sin\left(\frac{n\pi\psi}{\psi^*}\right)\cos(m\phi) + h_{32}\left[-\frac{(mC)}{rR\xi}\sin(m\phi)\sin\phi + \frac{C}{(r\xi)^2}\left(\frac{n\pi\gamma}{\psi^*}\right)^2\cos(m\phi)\right]\right\}\sin\left(\frac{n\pi\psi}{\psi^*}\right). \tag{43}$$

Accordingly, detailed signal contributions from various strain components and their modal voltages can be evaluated and significant components identified.

5. SENSOR SIGNALS OF NON-LINEAR TOROIDAL SHELLS

Distributed signals and the strain contributions of a distributed sensor layer laminated on a thin *linear* toroidal shell of revolution were defined previously. Distributed signals and modal voltages of a sensor layer and neurons laminated on a *non-linear* toroidal shell are defined in this section. As discussed previously, based on the von Karman geometrical non-linearity, the bending strains of the non-linear toroidal shell remain identical to the linear case. However, a quadratic effect of the non-linear transverse displacement is added to the membrane strains [18]:

$$s^{\circ}_{\phi\phi} = \frac{1}{r}\left(\frac{\partial u_\phi}{\partial\phi} + u_3\right) + \frac{1}{2}\left(\frac{\partial u_3}{\partial\phi}\right)^2, \tag{44}$$

$$s^{\circ}_{\chi\chi} = \frac{1}{r\xi}\left(-u_\phi\gamma\sin\phi + \frac{\partial u_\chi}{\partial\chi} + u_3\gamma\cos\phi\right) + \frac{1}{2}\left(\frac{\partial u_3}{\partial\chi}\right)^2. \tag{45}$$

Assume that the geometric non-linearity is small and its influence on natural modes is insignificant. Substituting the mode shape functions defined for the toroidal shell with the Denell–Mushtari–Vlasov assumption and simplifying gives the strain-mode shape function relations:

$$\frac{1}{2}\left(\frac{\partial u_3}{\partial\phi}\right)^2 = \frac{1}{2}(mC)^2\sin^2\left(\frac{n\pi\psi}{\psi^*}\right)\sin^2(m\phi), \tag{46}$$

$$\frac{1}{2}\left(\frac{\partial u_3}{\partial\chi}\right)^2 = \frac{1}{2}C^2\left(\frac{n\pi\gamma}{\psi^*}\right)^2\cos^2\left(\frac{n\pi\psi}{\psi^*}\right)\cos^2(m\phi), \tag{47}$$

$$s^{\circ}_{\phi\phi}(m,n) = \frac{(mA+C)}{r}\sin\left(\frac{n\pi\psi}{\psi^*}\right)\cos(m\phi) + \frac{1}{2}(mC)^2\sin^2\left(\frac{n\pi\psi}{\psi^*}\right)\sin^2(m\phi), \tag{48}$$

$$s^{\circ}_{\psi\psi}(m,n) = \frac{1}{r\xi}\left[-A\gamma\sin(m\phi)\sin\phi - B\left(\frac{n\pi\gamma}{\psi^*}\right)\cos(m\phi) + C\gamma\cos(m\phi)\cos\phi\right]\sin\left(\frac{n\pi\psi}{\psi^*}\right)$$

$$+\frac{1}{2}C^2\left(\frac{n\pi\gamma}{\psi^*}\right)^2\cos^2\left(\frac{n\pi\psi}{\psi^*}\right)\cos^2(m\phi). \tag{49}$$

The mnth modal sensing signals $[\phi^s_{mn}(\phi^*_a,\psi^*_a)]_{men}$ induced by the membrane strains, $[\phi^s_{mn}(\phi^*_a,\psi^*_a)]_{bend}$ contributed by the bending strains, the total signals $[\phi^s_{mn}(\phi^*_a,\psi^*_a)] = [\phi^s_{mn}(\phi^*_a,\psi^*_a)]_{men} + [\phi^s_{mn}(\phi^*_a,\psi^*_a)]_{bend}$, and the spatially distributed signals $[\phi^s_{mn}(\phi,\psi)]$ including the geometric non-linearity effect can be respectively defined as follows. Note that $[\phi^s_{mn}(\phi^*_a,\psi^*_a)]_{bend}$ is identical to the linear case.

$$[\phi^s_{mn}(\phi^*_a,\psi^*_a)]_{men} = h^s(h_{31}s^{\circ}_{\phi\phi} + h_{32}s^{\circ}_{\psi\psi})$$

$$= h^s\left(h_{31}\left[\frac{(mA+C)}{r}\sin\left(\frac{n\pi\psi}{\psi^*}\right)\cos(m\phi) + \frac{1}{2}(mC)^2\sin^2\left(\frac{n\pi\psi}{\psi^*}\right)\sin^2(m\phi)\right]\right.$$

$$+ h_{32}\left\{\frac{1}{r\xi}\left[-A\gamma\sin(m\phi)\sin\phi - B\left(\frac{n\pi\gamma}{\psi^*}\right)\cos(m\phi)\right.\right.$$

$$\left.+ C\gamma\cos(m\phi)\cos\phi\right]\sin\left(\frac{n\pi\psi}{\psi^*}\right)$$

$$\left.\left.+\frac{1}{2}C^2\left(\frac{n\pi\gamma}{\psi^*}\right)^2\cos^2\left(\frac{n\pi\psi}{\psi^*}\right)\cos^2(m\phi)\right\}\right), \tag{50}$$

$$[\phi^s_{mn}(\phi^*_a,\psi^*_a)]_{bend} = \frac{h^s(h+h^s)}{2}\left\{h_{31}\frac{(m^2C)}{r^2}\sin\left(\frac{n\pi\psi}{\psi^*}\right)\cos(m\phi)\right.$$

$$+ h_{32}\left[-\frac{(mC)}{rR\xi}\sin(m\phi)\sin\phi\right.$$

$$\left.\left.+\frac{C}{(r\xi)^2}\left(\frac{n\pi\gamma}{\psi^*}\right)^2\cos(m\phi)\right]\right\}\sin\left(\frac{n\pi\psi}{\psi^*}\right), \tag{51}$$

$$\phi^s_{mn}(\phi^*_a,\psi^*_a) = h^s\left\{h_{31}\left[\left[\frac{(mA+C)}{r} + \frac{(h+h^s)(m^2C)}{2r^2}\right]\sin\left(\frac{n\pi\psi}{\psi^*}\right)\cos(m\phi)\right.\right.$$

$$\left.+\frac{1}{2}(mC)^2\sin^2\left(\frac{n\pi\psi}{\psi^*}\right)\sin^2(m\phi)\right]$$

$$+ h_{32}\left[\left(\left[-\frac{A\gamma}{r\xi} - \frac{(h+h^s)(mC)}{2rR\xi}\right]\sin(m\phi)\sin\phi\right.\right.$$

$$\left.+\left[-B\left(\frac{n\pi\gamma}{\psi^*}\right) + \frac{C(h+h^s)}{2(r\xi)^2}\left(\frac{n\pi\gamma}{\psi^*}\right)^2\right]\cos(m\phi) + (C\gamma)\cos(m\phi)\cos\phi\right)$$

$$\left.\left.\times\sin\left(\frac{n\pi\psi}{\psi^*}\right) + \frac{1}{2}C^2\left(\frac{n\pi\gamma}{\psi^*}\right)^2\cos^2\left(\frac{n\pi\psi}{\psi^*}\right)\cos^2(m\phi)\right]\right\}, \tag{52}$$

$$\phi^s_{mn}(\phi,\psi) = \frac{h^s}{S^e}\int_\phi\int_\psi \left\{ h_{31}\left[\left[\frac{(mA+C)}{r} + \frac{(h+h^s)(m^2C)}{2r^2}\right]\sin\left(\frac{n\pi\psi}{\psi^*}\right)\cos(m\phi)\right.\right.$$

$$\left. + \frac{1}{2}(mC)^2\sin^2\left(\frac{n\pi\psi}{\psi^*}\right)\sin^2(m\phi)\right]$$

$$+ h_{32}\left[\left(\left[-\frac{A\gamma}{r\xi} - \frac{(h+h^s)(mC)}{2rR\xi}\right]\sin(m\phi)\sin\phi\right.\right.$$

$$\left. + \left[-B\left(\frac{n\pi\gamma}{\psi^*}\right) + \frac{C(h+h^s)}{2(r\xi)^2}\left(\frac{n\pi\gamma}{\psi^*}\right)^2\right]\cos(m\phi) + (C\gamma)\cos(m\phi)\cos\phi\right)$$

$$\left.\left. \times \sin\left(\frac{n\pi\psi}{\psi^*}\right) + \frac{1}{2}C^2\left(\frac{n\pi\gamma}{\psi^*}\right)^2\cos^2\left(\frac{n\pi\psi}{\psi^*}\right)\cos^2(m\phi)\right]\right\} r^2(1+\gamma\cos\phi)\,\mathrm{d}\phi\,\mathrm{d}\psi. \tag{53}$$

Thus, distributed modal voltages and signal contributions of non-linear toroidal shells can be evaluated accordingly. Again, the sensing signals are calculated based on "small" geometric non-linearity of toroidal shells, such that the mode shape functions remain uninfluenced.

6. MODAL VOLTAGES AND SIGNAL ANALYSIS

Recall that the signal generation is a function of strains induced in the sensor layer at various modal oscillations of the toroidal shells. Modal voltages and signal components associated with various strain components are analyzed in this section. It is assumed that the piezoelectric constants h_{31} and h_{32} are the same, the radius ratio $R/r = 4$, and the modal amplitudes A_{mn}, B_{mn}, and C_{mn} are assumed to be unity. Thus, the modal signals are normalized with respect to the modal amplitudes, *per se*. Note that the modal amplitudes A_{mn}, B_{mn}, and C_{mn} fluctuate at different modes and their relative amplitudes vary with respect to the shell geometries and/or sizes in reality. Accordingly, the following modal voltage plots and various signal components only provide *qualitative* information. *Quantitative* modal voltages can be inferred only if the "true" modal amplitudes of the toroidal shell are well defined. This model amplitude influence on the *non-linear*

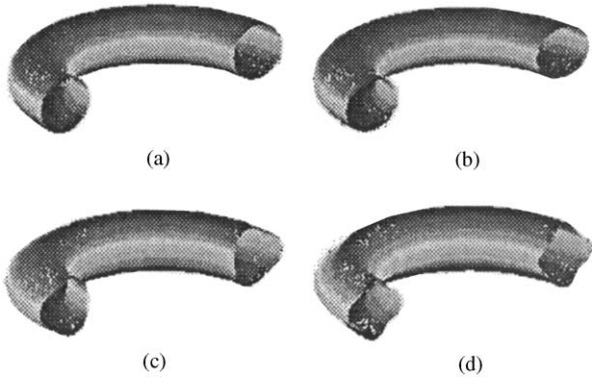

Figure 2. Signal distributions induced by the meridional membrane strains: (a) $m = 1$, (b) 2, (c) 3, (d) 4.

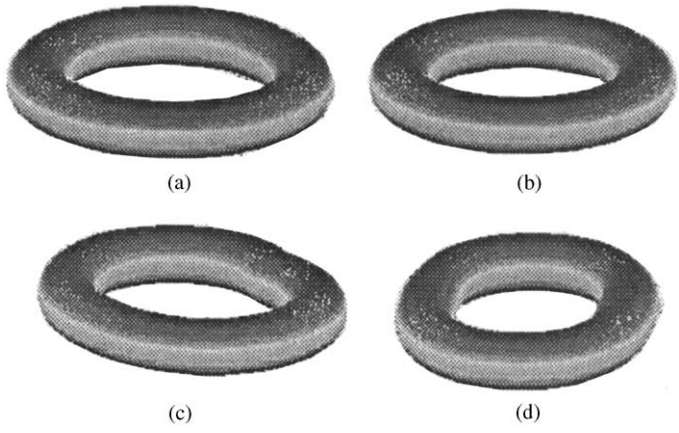

Figure 3. Signal distributions induced by the circumferential membrane strains: (a) $n = 1$, (b) 2, (c) 3, (d) 4.

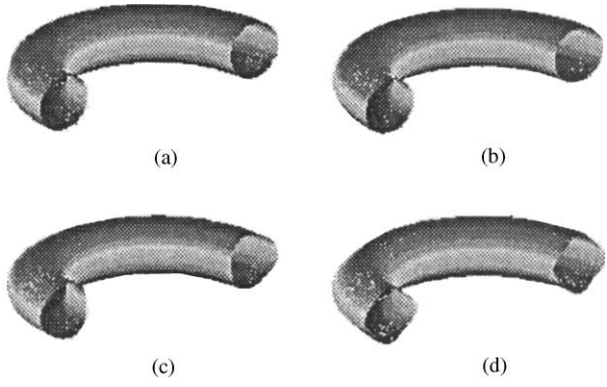

Figure 4. Signal distributions induced by the meridional bending strains: (a) $m = 1$, (b) 2, (c) 3, (d) 4.

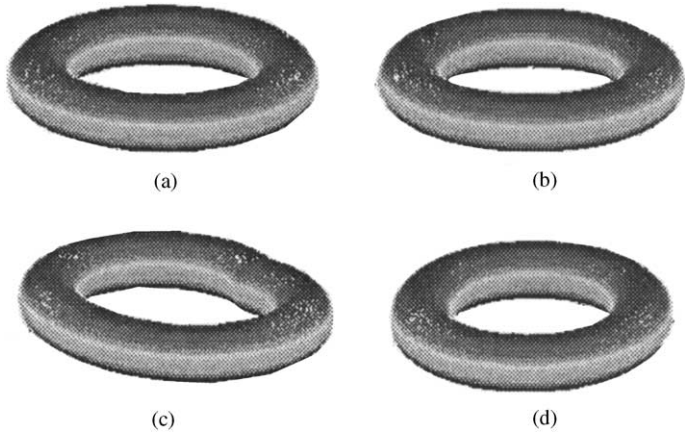

Figure 5. Signal distributions induced by the circumferential bending strains: (a) $n = 1$, (b) 2, (c) 3, (d) 4.

component is significant, since there is a quadratic term involved in the expression, due to the von Karman geometric non-linearity. The true signals of the non-linear component are usually small when the true modal amplitudes are considered.

Figures 2–5 illustrate the distributed modal signal components of the toroidal shell respectively induced by the meridional membrane strains, the circumferential membrane strains, the meridional bending strains, and the circumferential bending strains. In order to illustrate the individual modal effect in a specific direction, only one wave number is allowed to change from 1 to 4, while the other wave number is fixed. For example, m varies from 1 to 4, while n is fixed at 1, i.e., ($m = 1-4$, $n = 1$). Figures 2 and 4 illustrate the signal variations ($m = 1-4$, $n = 1$) in the meridional direction ϕ on the open cross-sections; Figures 3 and 5 show the circumferential signal variations ($m = 1$, $n = 1-4$) of the

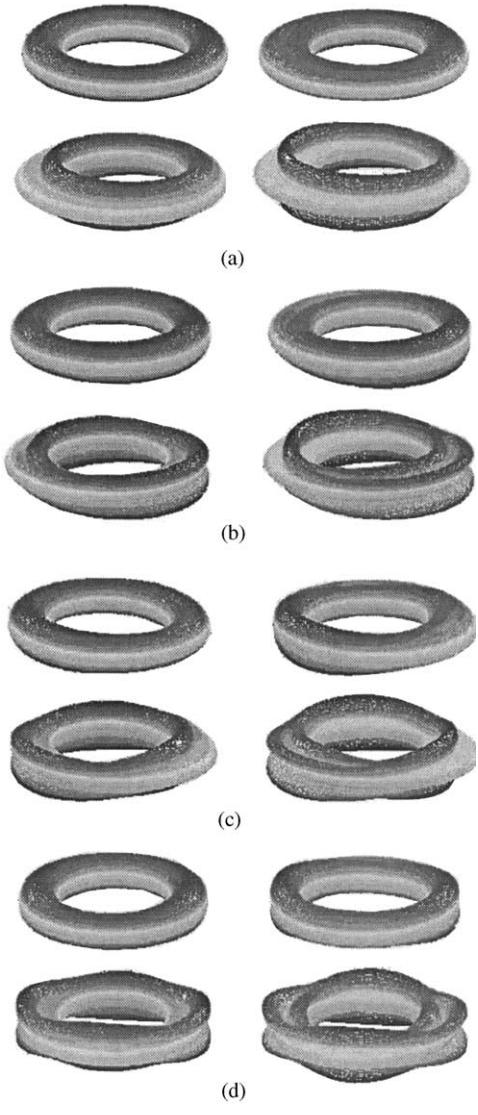

Figure 6. Modal voltage distributions contributed by the membrane strains: (a) modes ($m = 1-4$, $n = 1$); (b) modes ($m = 1-4$, $n = 2$); (c) modes ($m = 1-4$, $n = 3$); (d) modes ($m = 1-4$, $n = 4$).

toroidal shell. Note that the top left is "1", the top right is "2", the bottom left is "3", and the bottom right is "4" in the following modal signals. Furthermore, modal voltages ($m = 1-4$, $n = 1-4$) contributed by the total membrane strain components and those contributed by the total bending components are presented in Figures 6 and 7. There are a total of 16 modal voltage components to illustrate the signal variations at various natural modes in each plot. Again, the modes are arranged from the top left to the top right, and then from the bottom left to the bottom right in these distributed modal signals. These modal voltages and their signal components clearly illustrate distinct modal characteristics. Again, these signal distributions are calculated based on the infinite number of infinitesimally small sensor electrodes—neurons, such that the microscopic distributed signal behaviors can be observed clearly.

Again, these modal voltage plots and various signal components only provide *qualitative* spatial distribution of sensing signals. *Quantitative* modal voltages can be

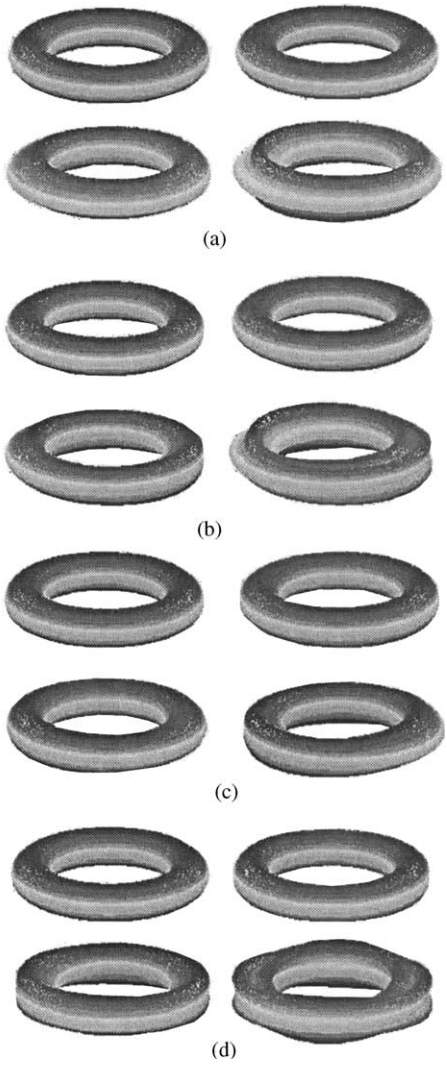

Figure 7. Modal voltage distributions contributed by the bending strains: (a) modes ($m = 1-4$, $n = 1$); (b) modes ($m = 1-4$, $n = 2$); (c) modes ($m = 1-4$, $n = 3$); (d) modes ($m = 1-4$, $n = 4$).

inferred only if the "true" modal amplitudes and geometries of the toroidal shell are well defined. Analytical solutions also suggest that the membrane-induced signal component is much larger than the bending-induced signal component. The meridional membrane component is larger than the circumferential component.

Detailed two-dimensional distributed signals in the meridional and circumferential directions are also calculated and plotted. Figure 8 illustrates the signals ($m = 1-4$, $n = 1$) and ($m = 1$, $n = 1-4$) respectively induced by the meridional and circumferential membrane strains of a *linear* toroidal shell; Figure 9 illustrates the signals ($m = 1-4$, $n = 1$) and ($m = 1$, $n = 1-4$) induced by the meridional and circumferential bending strains of the *linear* toroidal shell. Figures 10 and 11 respectively illustrate the distributed signals induced by the meridional and circumferential membrane strains of a *non-linear* toroidal shell. For convenience, a reference point is used in the circumferential plots. Note that the signals

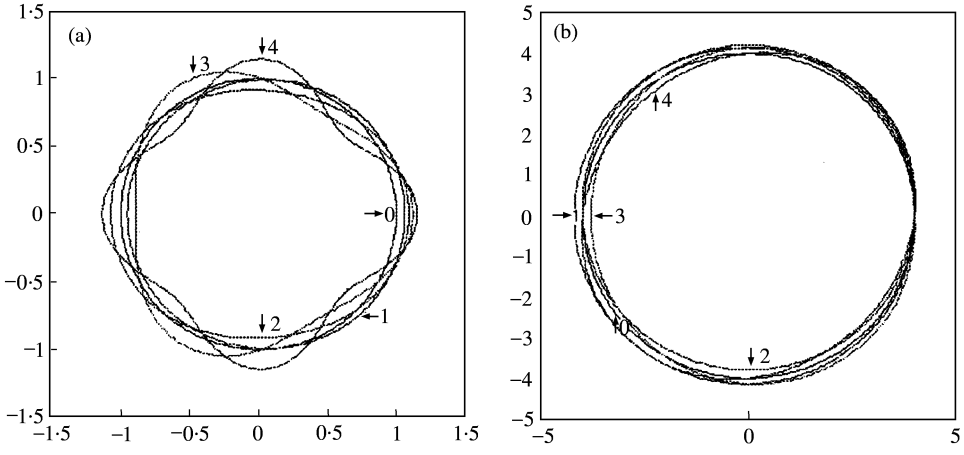

Figure 8. Signal distributions ($m = 1-4$, $n = 1$) and ($m = 1$, $n = 1-4$), respectively, induced by the meridional (a) and the circumferential (b) membrane strains: (a) 0, toroidal shell; 1, first mode; 2, second mode; 3, third mode; 4, fourth mode; (b) 0, toroidal shell; 1, first mode; 2, second mode; 3, third mode; 4, fourth mode.

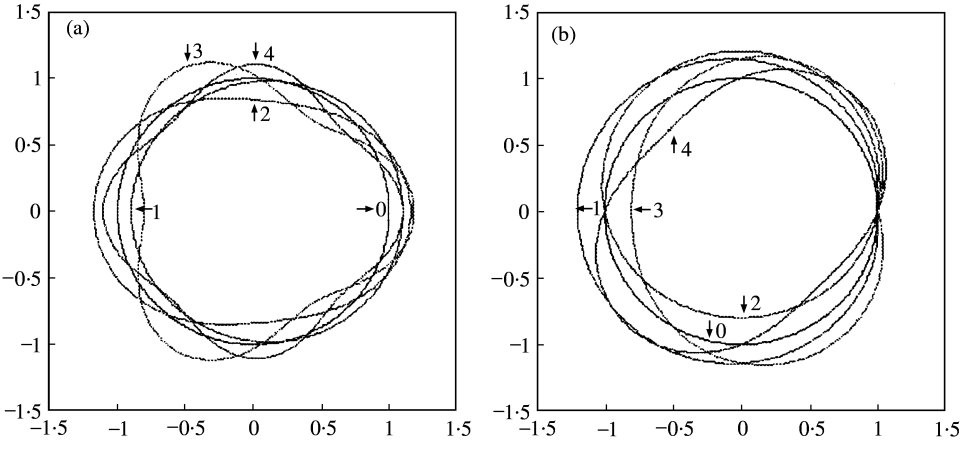

Figure 9. Signal distributions ($m = 1-4$, $n = 1$) and ($m = 1$, $n = 1-4$), respectively, induced by the meridional (a) and circumferential (b) bending strains: (a) 0, toroidal shell; 1, first mode; 2, second mode; 3, third mode; 4, fourth mode; (b) 0, toroidal shell; 1, first mode; 2, second mode; 3, third mode; 4, fourth mode.

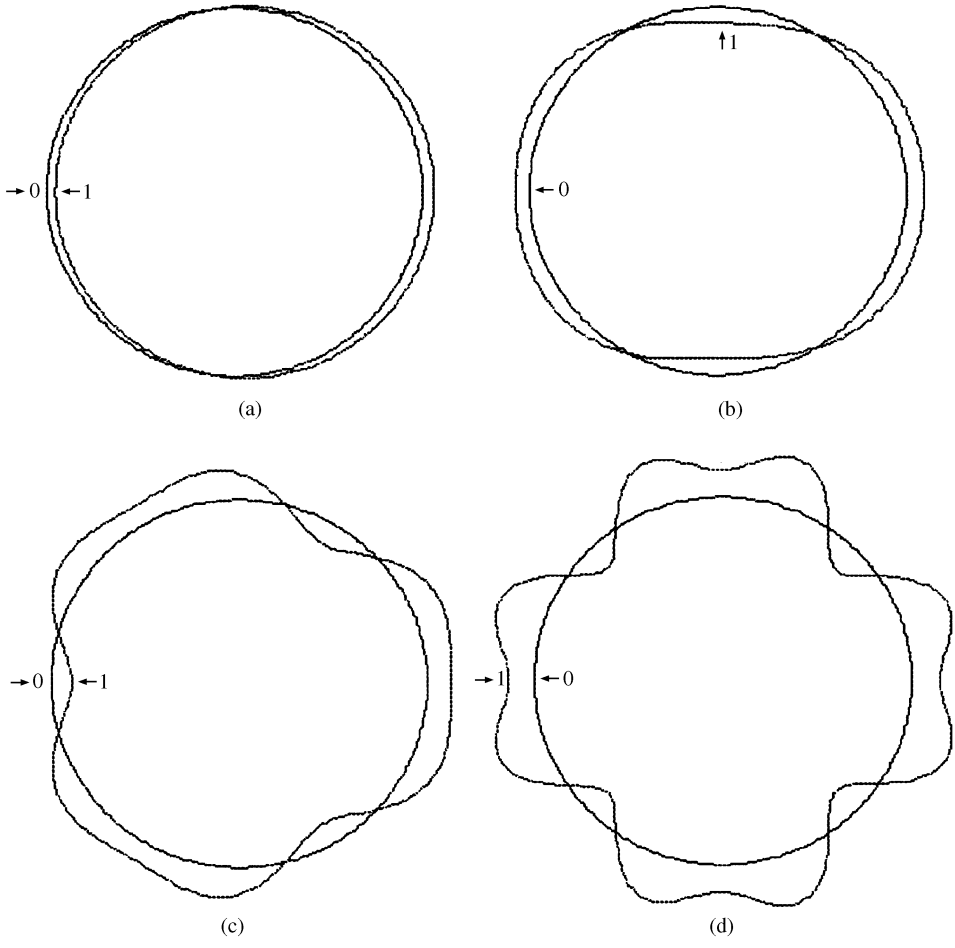

Figure 10. Signal distributions ($m = 1-4$, $n = 1$) induced by the meridional membrane strains of a non-linear toroidal shell: (a) first mode; (b), second mode; (c), third mode; (d), fourth mode. (0, shell; 1, modal signals)

induced by the meridional component are more significant than those induced by the circumferential component, because the strain levels are higher in the meridional direction. The signal distribution patterns, Figures 10 and 11, of the non-linear toroidal shell are different from those, Figure 8, of the linear toroidal shell, due to the quadratic non-linear term in the membrane strains. The signal distributions, Figure 9, induced by the bending strains remain identical for both linear and non-linear toroidal shells.

7. CONCLUSIONS

Toroidal shells belong to the shells of revolution family, in which the shell surfaces are formed based on full or partial rotations of specified lines or curves. Dynamics, measurement, and control are critical issue for advanced precision toroidal shell structures and components. Dynamic sensing signals and their distributed characteristics of spatially distributed sensors or neurons laminated on toroidal shell structures are investigated in this study. Mathematical models of linear and non-linear toroidal shells were established based on the thin shell theory and the von Karman geometric non-linearity assumptions. Modal-dependent distributed signals and detailed signal components of spatially

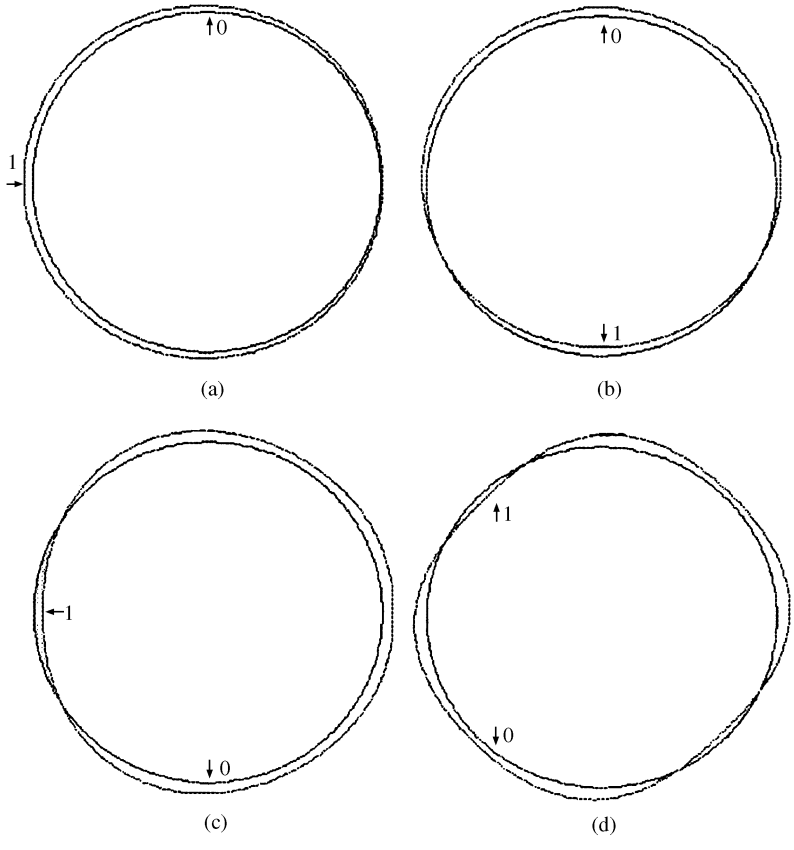

Figure 11. Signal distributions ($m = 1$, $n = 1-4$) induced by the circumferential membrane strains of a non-linear toroidal shell: (a) first mode; (b) second mode; (c) third mode; (d) fourth mode. (0, shell; 1, modal signals)

distributed sensors or neurons were defined based on the simplified mode shape functions defined by the Donnell–Mushtari–Vlasov theory. Detailed modal signal distributions depend on variations of the meridional and circumferential membrane/bending strains, defined by the direct piezoelectricity, the Gauss theorem, the Maxwell principle and the open-circuit assumption. Accordingly, with the analytical solutions, various distributed signals, modal voltages, and contributing signal components of distributed thin-film sensors and neurons laminated on linear and non-linear toroidal shells were evaluated quantitatively. Parametric studies of distributed modal voltages and signal distributions suggest that the dominating signal component results from the meridional membrane strains, rather than the circumferential membrane strains. The signals contributed by the bending components are relatively insignificant, as compared with the membrane counterparts. Signal distributions basically reveal distinct modal characteristics of toroidal shells. Analysis data also indicate that the distributed sensor layout of this toroidal shell consists of meridionally laminated strips that would provide the best measurement effect at the least material cost. This analysis also suggests that distributed signals and dominating signal components of toroidal shells depend on not only materials and dimensions, but also boundary conditions, natural modes, sensor locations, modal strain components, etc. As these design parameters change, the effective distributed sensor layouts or signal patterns would also change.

ACKNOWLEDGMENTS

This research was supported, in part, by a grant (F49620-98-1-0467) from the Air Force Office of Scientific Research (Project Manager: Brian Sanders). This support is gratefully acknowledged.

REFERENCES

1. F. Zhang and F. Redekop 1992 *Computers and Structures* **43**, 1019–1028. Surface loading of a thin-walled toroidal shell.
2. S. K. Naboulsi, A. N. Palazotto and J. M. Greer Jr 2000 *Journal of Aerospace Engineering* **13**, 110–121. Static–dynamic analyses of toroidal shells.
3. A. Y. T. Leung and T. C. Kwok 1995 *Thin-Walled Structures* **21**, 43–64. Dynamic stiffness analysis of toroidal shells.
4. G. D. Galletly and D. A. Galletly 1996 *Thin-Walled Structures* **26**, 195–212. Buckling of complex toroidal shell structures.
5. D. Redekop, B. Xu and Y. M. Zhang 1999 *International Journal of Pressure Vessels and Piping* **76**, 575–581. Stability of a toroidal fluid-containing shell.
6. F. J. M. Q. Melo and P. M. S. T. De Castro 1997 *Journal of Strain Analysis for Engineering Design* **32**, 47–59. Linear elastic stress analysis of curved pipes under generalized loads using a reduced integration finite ring element.
7. D. W. Huang, D. Redekop and B. Xu 1997 *Composite Structures* **63**, 465–473. Natural frequencies and mode shapes of curved pipes.
8. A. Y. T. Leung and T. C. Kwok 1994 *Thin-Walled Structures* **19**, 317–332. Free vibration analysis of a toroidal shell.
9. H. S. Tzou 1993 *Piezoelectric Shells (Distributed Sensing and Control of Continua*). Boston: Kluwer Academic Publishers.
10. H. S. Tzou, J. P. Zhong and M. C. Natori 1993 *American Society of Mechanical Engineers Journal of Vibration and Acoustics* **115**, 40–46. Sensor mechanics of distributed shell convolving sensors applied to flexible rings.
11. H. S. Tzou, Y. Bao and V. B. Venkayya 1996 *Journal of Sound and Vibration* **197**, 207–224. Study of segmented transducers laminated on cylindrical shells, Part-1: sensor patches.
12. H. S. Tzou, V. B. Venkayya and J. J. Hollkamp 1998 in *Dynamics and Control of Distributed Systems* (H. S. Tzou and L. A. Bergman, editors), 304–370. Cambridge: Cambridge University Press. Orthogonal sensing and control of continua with distributed transducers.
13. H. S. Tzou, Y. Bao and Y. Zhou 1997 *American Society of Mechanical Engineers Transactions, Journal of Vibration and Acoustics* **119**, 374–389. Nonlinear piezothermoelasticity and multi-field actuations, Part-1: nonlinear anisotropic piezothermoelastic shell laminates; Part-2: control of nonlinear buckling and dynamics.
14. H. S. Tzou 1992 in *Precision Sensors, Actuators, and Systems* (H. S. Tzou and T. Fukuda, editors), 175–218. Dordrecht: Kluwer Academic Publishers. Thin-layer distributed piezoelectric neurons and muscles: electromechanics and applications.
15. L. H. He, C. W. Lim and A. K. Soh 2000 *Acta Mechanica* **145**, 189–204. Three-dimensional analysis of an antiparallel piezoelectric bimorph.
16. Z. Cheng, C. W. Lim and S. Kitipornchai 2000 *International Journal of solids and Structures* **37**, 3153–3175. Three-dimensional asymptotic approach to inhomogeneous and laminated piezoelectric plates.
17. A. W. Leissa 1973 *NASA Report SP*-288. *Vibration of shells*.
18. H. S. Tzou and R. J. Yang 2000 *Journal of Theoretical and Applied Mechanics* **38**, 623–644. Nonlinear piezothermoelastic shell theory applied to control of variable-geometry shells.